Available online at www.sciencedirect.com
ScienceDirect
Proceedings of the Combustion Institute 000 (2020) 1–9
Proceedings of the Combustion Institute
www.elsevier.com/locate/proci

Autoignition of reacting mixtures at engine-relevant conditions using confined spherically expanding flames ☆,☆☆

Robert Lawson [a,*], Vyaas Gururajan [b], Ashkan Movaghar [a], Fokion N. Egolfopoulos [a]

[a] *Department of Aerospace and Mechanical Engineering, University of Southern California, Los Angeles, CA, 90089-1453, USA*
[b] *Energy Systems, Argonne National Laboratory, Lemont, IL, 60439, USA*

Received 5 November 2019; accepted 10 June 2020
Available online xxx

Abstract

Propagation of a confined spherically expanding flame induces isentropic compression that can culminate in autoignition and/or detonation under conducive thermodynamic conditions. This relatively simple technique measures a distinct 'characteristic ignition delay time' and complements other established approaches such as the rapid compression machine and shock tube. The present study details this methodology by examining the autoignition characteristics of dimethyl-ether/oxygen/nitrogen/helium reactive mixtures for equivalence ratios of 0.6 and 0.9, an initial temperature of 468 K, and initial pressures of 3 to 6 atm. The experimental results display the classic two-stage ignition typical of dimethyl-ether oxidation at low-temperatures with first-stage ignition occurring at approximately 3.6 times the initial pressure. To aid in the interpretation of the experimental results, two numerical models were used: a zero-dimensional batch reactor model, which accepts experimental pressure-time history and calculates the sensitivities of characteristic ignition delay times to kinetics, and a low Mach number, Lagrangian one-dimensional code that was developed to model both flame propagation and end-gas autoignition. Simulation results were shown to adequately capture the physics of unsteady flame propagation, end-gas autoignition, and the controlling reactions of the latter. It was found also that under certain conditions the behavior of first and second ignition stages could be modified by unsteady pressure effects.

Keywords: Laminar flames; End-gas; Autoignition; Low-temperature chemistry; Spherically expanding flames

☆ Colloquium Topic Area: Laminar Flames
☆☆ Submitted for presentation at the 38th International Symposium on Combustion, Adelaide, Australia, January 24th – January 29th, 2021.

* Corresponding author.
E-mail address: rlawson@usc.edu (R. Lawson).

https://doi.org/10.1016/j.proci.2020.06.224
1540-7489

1. Introduction

Knock has been one among the major limitations in gasoline engine technology towards achieving higher efficiencies and has been the motivation of numerous studies. Experimental investigations have been performed using shock tubes (ST) (e.g., [1]), rapid compression machines (RCM) (e.g., [2]), and motored engines. The strength of STs and RCMs lie in their capacity to attain high thermodynamic conditions (400–3000 K, 2–100 bar) coupled with laser and optical diagnostics for ignition delay time (IDT) measurement, speciation time-history, reaction rate measurements, and knock studies. As described by Donovan et al. [3], the key desirable factors worth considering in an experimental study of autoignition phenomena are ample test times, high pressures and temperatures, good flow field and measurement access, for which the aforementioned duly satisfy.

Confined spherically expanding flames (CSEFs) employed for the measurement of laminar flame speeds (S_u^o) at high pressures and temperatures was pioneered by Lewis and von Elbe [4] and also offer acomplementary low-cost approach to yield insight into knocking phenomena as first suggested by Hu and Keck [5]. Their experimental investigations of C_4–C_8 alkanes demonstrated that a CSEF acts as a "piston" in that, the heat release of the propagating flame serves to increase the pressure homogeneously in the entire volume of confinement. Thus, the isentropic compression of the end-gas for particular initial conditions, could bring about autoignition under variable pressure conditions that closely mimics the engine behavior [5].

In addition, the absence of any movable parts reduces the maintenance and operating cost. The available experimental test times for compression range from ~25–50 ms and compression ratios ~5–8, sufficient to promote chemical induction and radical initiation processes at low-temperatures. Achieving this requires tailoring S_u^o through mixture conditions such that the timescales of flame propagation become comparable to unburnt gas chemical reaction.

There are only two experimental studies that used CSEFs to investigate autoignition systematically [6,7]. The limited use of the initial proposition by Hu and Keck [5] is mainly due to the lack of high-fidelity tools that could simultaneously simulate, the phenomena of flame propagation and auto-ignition, which is a stringent requirement for chemical kinetic model development. In other studies such as [8–11], the autoignition via flame-induced compression has also been investigated.

The goal of the present investigation is to revisit the original proposition of Hu and Keck [5] by experimentally characterizing end-gas autoignition and interpreting these observables using direct numerical simulation (DNS) tools. The canonical nature of the experiment suits the use of a 1-D low Mach number reacting flow code to accurately model all the relevant physics: flame propagation, heat loss at the walls, and end-gas autoignition. The method is demonstrated by using reactive DME-oxygen-inert-mixtures, known to exhibit negative temperature coefficient (NTC) behavior.

2. Experimental approach

All CSEF experiments and pertinent procedures were performed in a heated and entirely spherical chamber as described in [12,13]. Distinction is hereby made with another spherically expanding flame configuration (usually under constant pressure) where the flame radius trajectory is obtained using high speed photography while this method utilizes only the monitored pressure rise in the vessel without any optical access [12,14]. All results and discussions presented herein will focus on the latter. The dynamic pressure transducer was calibrated at 468 K and 0–500 psi range to reduce the pressure-time [P, t] uncertainty (± 0.7 psi) [12] with the data being acquired at 100 kHz. The initial temperature is read with an Omega controller (CN9110A) with an uncertainty of ± 3 K. All gasses had purities > 99.5%. The experimental data and with corresponding uncertainties shown are tabulated in the Supplementary Material 1 (SPM1).

End-gas autoignition was investigated using DME (CH_3OCH_3) flames with initial thermodynamic conditions, mole fraction (X_i) compositions and initial adiabatic flame temperatures (T_{ad}) as listed in Table 1. The mixture dilution of $He/N_2 = 70/30$ on a molar basis was used with experiments conducted at an initial temperature $T_o = 468$ K and various initial pressures (P_o).

3. Modeling approach

3.1. End-gas autoignition

The time evolution of the unburned gas during isentropic compression was modeled using a recently developed 0-D adiabatic batch reactor model

Table 1
Summary of thermodynamic conditions investigated.

Mixture	ϕ	T_{ad} (K)	P_o (atm)	$X_{CH3OCH3}$	X_{O2}	X_{N2}	X_{HE}
1	0.9	1950	3,4,5,6	0.032967	0.109890	0.257143	0.60000
2	0.6	1925	3,4,5,6	0.033009	0.165047	0.240583	0.561361

Please cite this article as: R. Lawson, V. Gururajan and A. Movaghar et al., Autoignition of reacting mixtures at engine-relevant conditions using confined spherically expanding flames, Proceedings of the Combustion Institute, https://doi.org/10.1016/j.proci.2020.06.224

code (sensBVP) [15]. It is integrated with Cantera subroutines [16] and uses the experimental *P-t* trace as input in order to consistently compute a characteristic ignition delay time (τ_{CIDT}) by solving the energy and species equations as specified below (All variables are defined in the next section):

$$\frac{\partial T}{\partial t} = \frac{1}{\rho C p}\frac{dP}{dt} - \sum_{1}^{i} \omega_i h_i \tag{1}$$

$$\frac{\partial Y i}{\partial t} = \frac{\omega_i W_i}{\rho} \tag{2}$$

The sensBVP code calculates sensitivity of ignition delay times to rate coefficients by formulating the initial value problem (IVP) as a boundary value problem (BVP), thus obviating the brute force technique. The kinetic model of Zhao et al. [17] with 55 species and 290 reactions describing both low and high temperature chemistry was used and it has been validated for thermodynamic conditions relevant to this study.

3.2. Direct numerical simulations (DNS)

In order to directly simulate CSEF propagation and end-gas autoignition, a Lagrangian transient one-dimensional reacting flow code (LTORC) was developed in generalized coordinates. Lagrangian coordinates used here have been applied in other combustion-related studies (e.g., [18,19]), in order to eliminate numerical difficulties arising from the non-linear advective term in the energy and species equations. Other studies utilizing Lagrangian coordinates include the numerical calculations of S_u^o by Spalding [20], Dixon-Lewis [21], autoignition by Stauch et al. [22], and burning of droplets by Cho et al. [23]. The derivation and numerical application of the Lagrangian formulation can be found in [24]. The governing equations (in spherical coordinates) and boundary conditions are shown below:

$$\frac{\partial r}{\partial \psi} - \frac{1}{\rho r^2} = 0 \tag{3}$$

$$\frac{\partial P}{\partial \psi} = 0 \tag{4}$$

$$\rho C_p \frac{\partial T}{\partial t} + \dot{m}_o \frac{\partial T}{\partial \psi} - \rho \frac{\partial}{\partial \psi}\left(r^4 \rho \lambda \frac{\partial T}{\partial \lambda}\right) - \frac{\partial P}{\partial t} + \sum_{i=1}^{N} \dot{\omega}_i \Delta h^{\circ}_{f,i} + \rho^2 r^2 \frac{\partial T}{\partial \psi} \sum_{i=1}^{N} C_{p,i} Y_i V_i = 0 \tag{5}$$

$$\rho \frac{\partial Y_i}{\partial t} + \dot{m}_o \frac{\partial Y_i}{\partial \psi} + \rho \frac{\partial}{\partial \psi}\left(r^2 \rho Y_i V_i\right) - \left(W_i \dot{\omega}_i\right) = 0 \tag{6}$$

$$\left(\frac{\partial T}{\partial \psi}\right)_{r=0} = 0, \left(\frac{\partial Y_i}{\partial \psi}\right)_{r=0} = 0 \tag{BC1}$$

$$Adiabatic: \left(\frac{\partial T}{\partial \psi}\right)_{r=R} = 0, \; Non-adiabatic: (T)_{r=R} = T_{wall}, V_i = 0 \tag{BC2}$$

with:

r - spatial location
t - time
h_i – specific enthalpy of species
R - domain length
ρ - mixture density
P - thermodynamic pressure
C_p- bulk specific heat capacity at constant pressure
T - temperature
λ - thermal conductivity
Y_i - i^{th} species mass fraction
$\Delta h^{\circ}_{f,i}$ - standard enthalpy of formation
V_i - diffusion velocity (computed using a mixture-average formulation)
W_i - molecular mass
$\dot{\omega}_i$ - molar production rate
N - total number of species
ψ - Lagrangian variable

The method of lines approach is used to isolate temporal and spatial derivatives, the latter of which is discretized using finite differences. The system of equations is differential-algebraic and solved using IDA [25]. The fluid is treated as an ideal gas and the necessary thermodynamic, kinetic and transport calculations are carried out using Cantera [16]. To resolve the flame as it moves, a moving point density function constructed from hyperbolic tangent functions with high density at the flame at all times was used. Additional refinement was supplied at the wall (due to the thermal boundary layer there) and the origin (due to the occurrence of terms proportional to the square of the radius in the governing equations). Grid refinement is accompanied by third order monotone upwind interpolation from variables on the old grid to the new one. Additional details of the code and governing equations can be found in Supplementary Material 2 (SPM2), Section 1 while the simulated pressure results are tabulated in Supplementary Material 3 (SPM3). The source code for LTORC can be downloaded from [26].

A spherical domain of radius $R = 10.16$ cm was used with a non-adiabatic wall, corresponding to the experiments. X_o, P_o and T_o are as specified in Table 1. A small ignition kernel (< 5% of the domain volume) comprising a chemically equilibrated composition was used to initiate the flame.

Please cite this article as: R. Lawson, V. Gururajan and A. Movaghar et al., Autoignition of reacting mixtures at engine-relevant conditions using confined spherically expanding flames, Proceedings of the Combustion Institute, https://doi.org/10.1016/j.proci.2020.06.224

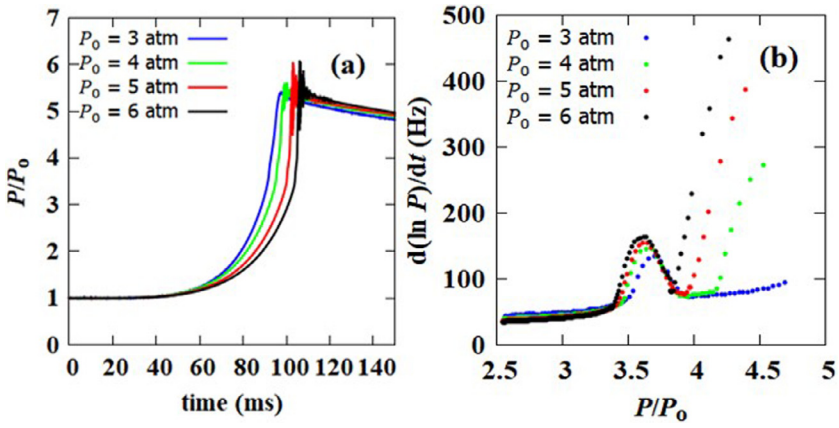

Fig. 1. Experimental results for Mixture 1: (a) temporal evolution of P and (b) d(ln$P$)/dt as a function of P/P_o for $P_o = 3$ atm (–), $P_o = 4$ atm (–), $P_o = 5$ atm (–), $P_o = 6$ atm (–).

4. Results and discussion

4.1. Characterization of end-gas autoignition

With the pressure trace being the only experimental observable, attention is devoted to any phenomena that could affect its measurement, such as for example flame-front instability and buoyancy.

For weakly burning CSEFs, the burned volume of gas is likely to lose its sphericity by becoming buoyant, a tendency promoted at higher pressures. To preclude this, the reactive mixtures were formulated by partially replacing N_2 with He, decreasing the molar specific heat of the diluent and raising T_{ad} resulting in increasing S_u^o. As such, S_u^os for freely propagating flames using the PREMIX code [27] were computed at the initial conditions in Table 1 to ensure buoyant-free flames. All the computed S_u^o values, shown in SPM2 Section 2, are greater than 35 cm/s guaranteeing a flame propagation unaffected by buoyancy.

The potential development of flame-front instabilities during propagation exists: thermo-diffusive and hydrodynamic [28] modes augment the mass burning rate by creating flame surface area. Helium was used for this reason as well as a diluent by increasing the mixture's Lewis number beyond unity [29], thus ensuring thermo-diffusional flame stability; high pressure S_u^o experiments (e.g., [12,13,30]) have employed this approach to achieve stable flames. It is worth noting also that the use of He, due to its higher heat capacity ratio, helps promote end-gas autoignition by attaining higher unburned gas mixture temperatures.

A typical experimental P-t trace and its gradient (dP/dt) obtained in a previous study in the absence of autoignition [12], is shown in SPM2 Section 3. When end-gas autoignition occurs (for conditions shown in Table 1) the P-t plot (Fig. 1a) exhibits pressure oscillations similar to previous studies [5-7]. The fractional rate of change of pressure (d(ln$P$)/dt) is plotted against P/P_o in Fig. 1b and the non-monotonic behavior is due to low-temperature kinetics similar to ignition caused by thermal boundary layers (TBL) [31].

The first-stage ignition, associated with a mild heat release, is manifested by the bump in d(ln$P$)/dt (occurring between $3 \leq P/P_o \leq 4$), while the violent second-stage ignition, associated with large heat release, corresponds to the rapid rise in d(ln$P$)/dt. After the point of autoignition, there is a generation of pressure oscillations due to the short duration of the increase in pressure compared to timescales of acoustic relaxation [32].

LTORC was used to model the entire experiment, capturing flame propagation, isentropic compression, end-gas reactivity upon compression, and near-wall TBL effects. Mixture 1 at $P_o = 6$ atm will be used to analyze the observed pressure response.

Directly after a hot ignition kernel is initiated at the origin ($r = 0$) at $t = 0$ ms, a flame propagates outwardly. During the initial stages, the unburned mixture is consumed almost isobarically with the temperature remaining at ~468 K. Following this, effective compression commences at $\sim \frac{R_f}{R_w} = 80\%$[12] as evident by the temporal evolution of temperature distribution in Fig. 2a at $r \sim 7$ cm up to 9.56 cm where the unburnt gas temperature (T_u) has risen to ~700 K with negligible low-temperature reactivity and/ or ignition. A TBL forms near the chamber wall [31] during flame propagation where heat loss occurs as seen by the insert in Fig. 2a.

For $t > 61.58$ ms and $r \sim 9.6$ cm, reactivity vigorously commences in the unburnt gas and there is a significant T_u jump to ~ 940 K, a manifestation of first-stage ignition. Further compression results in continuous temperature rise up to ~1040 K, at which point the second-stage ignition takes place

Please cite this article as: R. Lawson, V. Gururajan and A. Movaghar et al., Autoignition of reacting mixtures at engine-relevant conditions using confined spherically expanding flames, Proceedings of the Combustion Institute, https://doi.org/10.1016/j.proci.2020.06.224

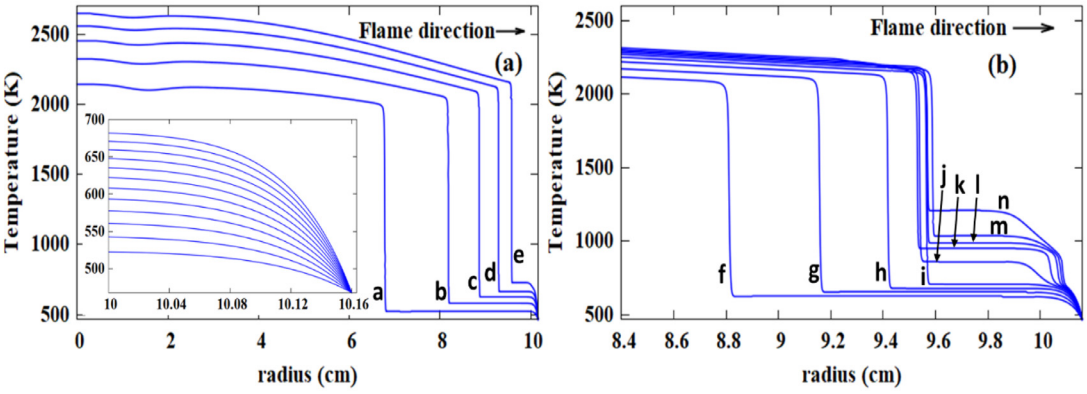

Fig. 2. Computed radial variation of T for Mixture 1 at $P_o = 6$ atm with corresponding time sequence (a) a - 36.12 ms, b - 47.84 ms, c - 54.31 ms, d – 58.60 ms, e – 61.80 ms, (b) f – 53.72 ms, g – 57.20 ms, h - 59.94 ms, i – 61.58 ms, j –61.96 ms, k - 62.2040 ms, l - 62.51 ms, m - 62.70 ms, n - 62.82 ms.

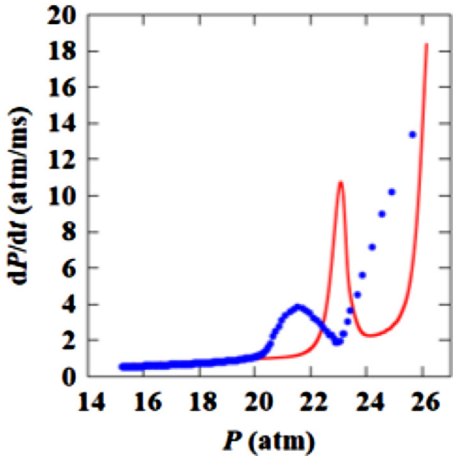

Fig. 3. Comparison of experimental (...) and computed (_) dP/dt as a function of P for Mixture 1 at $P_o = 6$ atm.

resulting in an exponential increase in temperature (Fig. 2b).

It was determined that the timescales of pressure rise in the end-gas when autoignition occurs are smaller than the acoustic relaxation timescales. Therefore, since the purpose of this work is to capture only the instant of autoignition, considerations of compressibility are safely negligible.

LTORC was found also to capture satisfactorily the phenomena of flame propagation and autoignition after comparing the experimental and computed dP/dt during compression for Mixture 1 at $P_o = 6$ atm. As shown in Fig. 3, there is agreement during the initial stages of flame propagation. However, when end-gas reactivity initiates significant discrepancies exist and could be caused by uncertainties in the kinetic model. To that end, the oxidation of DME has been studied in a jet-stirred reactor from low to high temperature (500–1100 K) conditions [33] and similar discrepancies were found using the present kinetic model as well as that of Burke et al. [34]. Analysis showed that the results are sensitive to the branching ratios involving the CH_2OCH_2OOH species. In spite of the discrepancies, the ability to qualitatively capture the trend by DNS provides encouraging evidence that the CSEF approach is viable towards probing autoignition phenomena at low temperatures.

4.2. Characteristic ignition delay time and sensitivity analysis

To further investigate the underlying chemistry of end-gas autoignition, the experimental P-t traces were fed as input into sensBVP, to determine the T_u, Y_i evolution and τ_{CIDT}. During low-temperature reactivity and ensuing first-stage ignition, the fuel breakdown undergoes a chain-branching sequence over a narrow thermodynamic range, generating OH radicals in the process while further augmenting the fuel's consumption along with attendant temperature rise. If low-temperature reactivity is absent and ignition does not occur (chemically frozen), the end-gas will only be isentropically compressed before being consumed entirely by the flame.

Fig. 4 depicts two computed results of the end-gas P-T_u of Mixture 1 at $P_o = 6$ atm. In both cases there is isentropic compression caused by the pressure rise, however in one, the end-gas reactivity has been suppressed and a deviation of the results initiates at $P \sim 23$ atm. At $T_u \sim 700$ K, low-temperature reactivity becomes significant resulting in first-stage ignition where the end-gas transitions to a different thermodynamic and chemical state. Despite the end-gas traversing the NTC region featuring a known decreased reactivity with increasing

Please cite this article as: R. Lawson, V. Gururajan and A. Movaghar et al., Autoignition of reacting mixtures at engine-relevant conditions using confined spherically expanding flames, Proceedings of the Combustion Institute, https://doi.org/10.1016/j.proci.2020.06.224

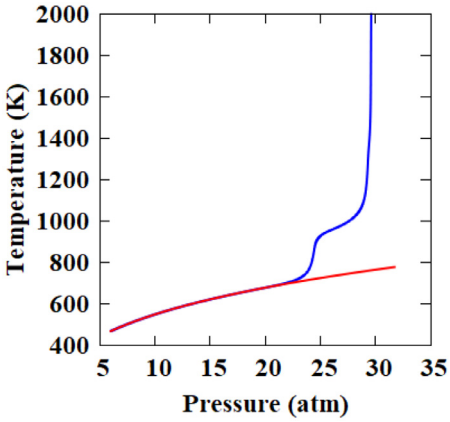

Fig. 4. Computed P-T_u functions for an unreactive (_) and reactive (_) end-gas for Mixture 1 at $P_o = 6$ atm.

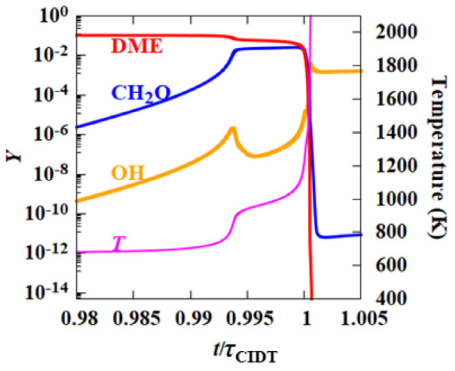

Fig. 5. Computed temperature profile, T (–) and DME (–), OH (–) and CH_2O (–) mass fractions in the unburned mixture as a function of the normalized time for Mixture 1 at $P_o = 6$ atm.

temperature, the simultaneous compression by CSEF results in the P-T_u rise. Finally, with considerable build-up of relevant chemical species promoting high temperature ignition, the second-stage occurs with an accompanying rapid temperature rise.

Compared to RCM, a key difference of the CSEF approach is that ignition is achieved in a time-varying thermodynamic (P, T_u) condition. Thus, a "traditional" ignition delay time (τ_{ign}) cannot be defined. Instead, a τ_{CIDT} is defined as the time elapsed from $t = 0$ to a point of rapid reaction phase leading to a temperature and pressure rise; τ_{CIDT} values from sensBVP for all Mixtures in Table 1 are displayed in SPM2 Section 4.

Formaldehyde (CH_2O), a strong marker of low-temperature reactivity [2,31,35], largely starts being produced in the end-gas. The CH_2O time-evolution shown in Fig. 5 also coincides with the initial temperature rise during first-stage ignition. At low-temperatures it is produced mainly from the β-scission of CH_3OCH_2 and CH_2OCH_2OOH

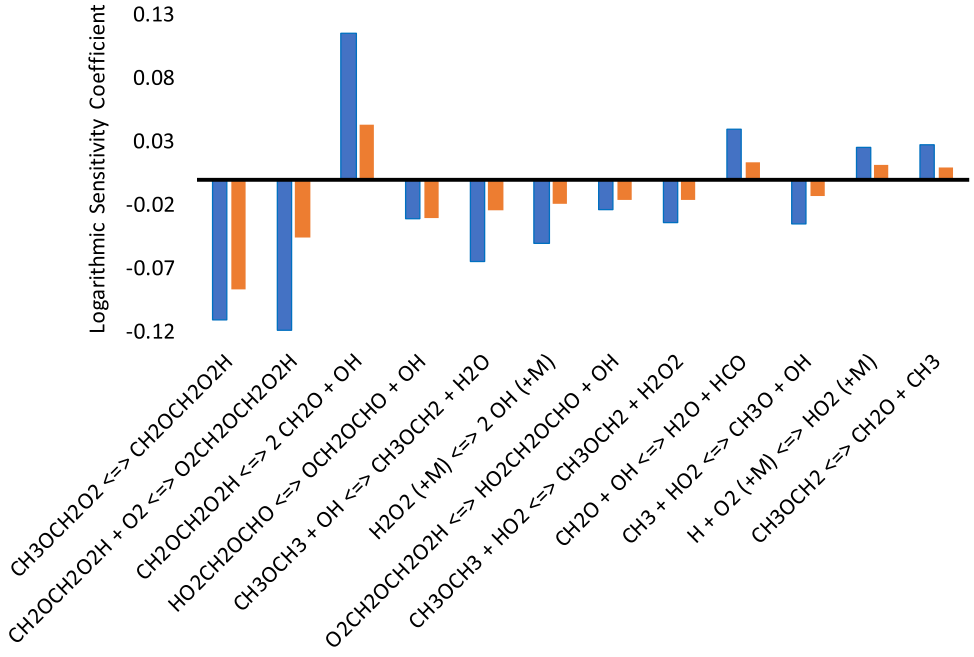

Fig. 6. Ranked LSC of τ_{CIDT} to kinetics for Mixture 1 at $P_o = 3$ (blue) and 6 atm (orange).

Please cite this article as: R. Lawson, V. Gururajan and A. Movaghar et al., Autoignition of reacting mixtures at engine-relevant conditions using confined spherically expanding flames, Proceedings of the Combustion Institute, https://doi.org/10.1016/j.proci.2020.06.224

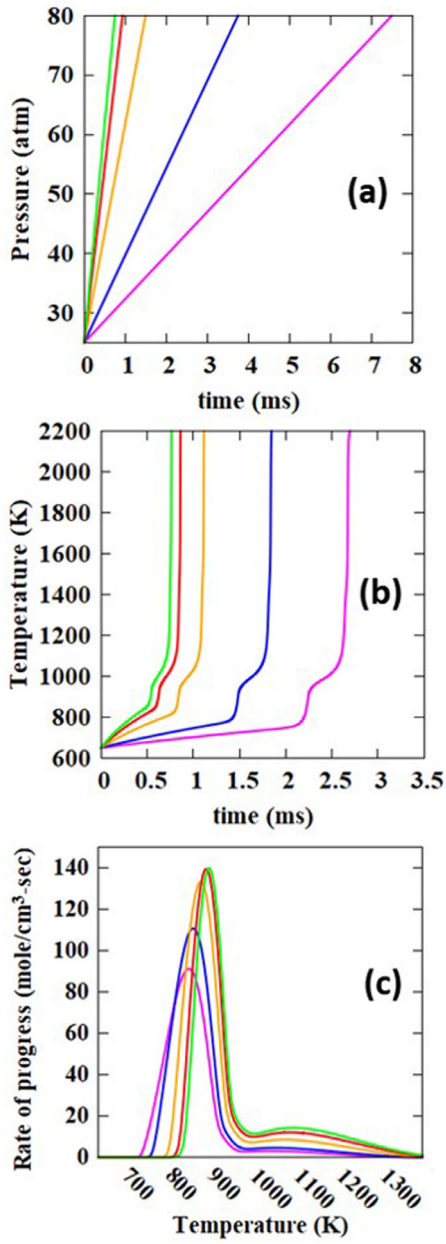

Fig. 7. **(a)** *P-t* history, (b) T_u-*t* variation and (c) Net rate of progress of $CH_3OCH_2O_2$ production from sensBVP for Mixture 1 at $P_o = 25$ atm, $T_{u,o} = 650$ K for $dP/dt = 7.33$ atm/ms (_), $dP/dt = 14.67$ atm/ms (_), $dP/dt = 36.67$ atm/ms (_), $dP/dt = 58.67$ atm/ms (_), $dP/dt = 73.33$ atm/ms (_).

which compete with other reactions leading to low-temperature chain branching.

At relatively higher temperatures and pressures, DME and CH_2O are rapidly consumed as OH build-up in the unburned mixture becomes prominent through $H_2O_2 + M \rightarrow OH + OH + M$ and results in second-stage ignition.

To assess the controlling reactions of end-gas autoignition, sensitivity analysis using sensBVP was performed. The ranked logarithmic sensitivity coefficients (LSC) for Mixture 1 at $P_o = 3$ and 6 atm is shown in Fig. 6. $CH_2OCH_2O_2H$ is consumed through two main pathways. The first being $CH_2OCH_2O_2H + O_2 \rightarrow O_2CH_2OCH_2O_2H$ with its product going through the following reaction steps $O_2CH_2OCH_2O_2H \rightarrow HO_2CH_2OCHO + OH$ and $HO_2CH_2OCHO \rightarrow OCH_2OCHO + OH$ releasing two OH radicals in a sequence that promotes low-temperature chain branching. The second being a β-scission reaction $CH_2OCH_2O_2H \rightarrow 2CH_2O + OH$ inhibits autoignition. β-scission of CH_3OCH_2 can also produce CH_2O and CH_3 radicals that inhibits autoignition. Thus, the competition between O_2 addition and β-scission reactions of $CH_2OCH_2O_2H$ at low-temperatures is largely responsible for the NTC behavior [34,36,37].

Similar to τ_{CIDT}, a characteristic first-stage ignition delay time (τ_{CIDT_1}) is also defined, but at the first-stage ignition point with sensitivity analysis performed subsequently for Mixture 1 at $P_o = 6$ atm. The results are compared with those of Fig. 6 in SPM2 Section 5 and as expected τ_{CIDT_1} is not sensitive to high-temperature kinetics.

4.3. Unsteady effects of pressure on kinetics

An important aspect of the CSEF approach is that autoignition initiates in the presence of dP/dt similar to piston engines. Furthermore, alkyl radical oxidation is highly dependent on the prevailing thermodynamic conditions. Thus, it becomes imperative to explore the effects of this transient pressure rise on kinetics at low temperatures.

To that end, four linear *P-t* traces shown in Fig. 7a for Mixture 1 at $T_o = 650$ K and $P_o = 25$ atm with increasing dP/dt to simulate different compression rates were fed into sensBVP to compute the T_u and Y_i evolution. The temperature history in Fig. 7b shows that with increasing dP/dt autoignition is affected notably. A kinetic analysis in Eq. (7) (shown below) involving DME H-abstraction ($CH_3OCH_3 + OH \rightarrow CH_3OCH_2 + H_2O$) and the first O_2 addition to CH_3OCH_2 ($CH_3OCH_2 + O_2 \leftrightarrow CH_3OCH_2O_2$) reactions and reveals that CH_3OCH_2 and thereby $CH_3OCH_2O_2$ formations are progressively being quenched by increasing dP/dt assuming constant temperature. More

Please cite this article as: R. Lawson, V. Gururajan and A. Movaghar et al., Autoignition of reacting mixtures at engine-relevant conditions using confined spherically expanding flames, Proceedings of the Combustion Institute, https://doi.org/10.1016/j.proci.2020.06.224

specifically,

$$\frac{dX_{CH3OCH2}}{dt} = K_{f,1}\frac{P}{R_uT}X_{CH3OCH3}X_{OH} - K_{f,2}\frac{P}{R_uT}X_{CH3OCH2}X_{O2} + K_{b,2}X_{CH3OCH2O2} - \frac{X_{CH3OCH2}}{P}\frac{dP}{dt} \quad (7)$$

dP/dt contributes a subtractive term proportional to the $X_{CH3OCH2}/P$. Thus, there is an acceleration towards high-temperature kinetics and second-stage ignition. It is also observed from the net rate of progress of $CH_3OCH_2 + O_2 \leftrightarrow CH_3OCH_2O_2$ in Fig. 7c that the production of $CH_3OCH_2O_2$ significantly decreases as dP/dt increases.

5. Concluding remarks

End-gas autoignition was investigated using the confined spherically expanding flame method for dimethyl-ether/O_2/N_2/He reactive mixtures. The distinctive features of the experimental pressure-time were highlighted through the pressure gradient, specifically during the compression region. Low-temperature ignition was identified by a 'bump' in the pressure gradient and high-temperature ignition by a rapid rise in pressure followed by pressure oscillations whose amplitude increased with higher initial pressure and for fuel lean conditions. For all experimental conditions, it was seen that first-stage ignition occurred approximately at 3.6 times the initial pressure.

A one-dimensional Lagrangian reacting flow code was developed to directly model the unsteady spherical flame propagation including isentropic compression, end-gas reactivity and autoignition at the same experimental conditions. The results showed that the expanding flame induced first-stage ignition during the compression followed immediately by the second-stage ignition. Furthermore, it was shown that the boundary layer shrunk with time, thereby minimizing the possibility of fluid mechanics interference with the adiabatic core.

Species and temperature time evolution were processed from the experimental pressure time history using a zero-dimensional code which in addition to calculating a characteristic ignition delay time along with mathematically rigorous sensitivity analysis to kinetics. It was found that this characteristic ignition delay is largely controlled by fuel-specific reactions, specifically, dimethyl-ether low-temperature chemistry. Additionally, the sensitivity to kinetics increases as the fuel mixture becomes leaner due to the increasing effect of oxygen in the low temperature chain branching.

The current study of autoignition using confined spherically expanding flames represents a complementary low-cost approach to obtain experimental data which can be modeled for reliable kinetic model validation under thermodynamic conditions relevant to engines. Coupled with numerical tools, the physics leading to engine knock can be reasonably explored to understand the controlling mechanisms.

Declaration of Competing Interest

The authors declare that they have no known competing financial interest or personal relationships that could have appeared to influence the work reported in this paper.

Acknowledgements

The work was supported by the Shell Global Solutions (Grants No. 61772258–134253 and 009762–00001) under the technical supervision of Drs. Allen Aradi and Tushar Bera. The authors appreciate the fruitful discussions with Prof. Jagannath Jayachandran.

Supplementary materials

Supplementary material associated with this article can be found, in the online version, at doi:10.1016/j.proci.2020.06.224.

References

[1] R.K. Hanson, D.F. Davidson, *Prog Energy Combust Sci* 44 (2014) 103–114.
[2] S.S. Goldsborough, S. Hochgreb, G. Vanhove, M.S. Wooldridge, H.J. Curran, C.J. Sung, *Prog Energy Combust Sci* 63 (2017) 1–78.
[3] M.T. Donovan, X. He, B.T. Zigler, T.R. Palmer, M.S. Wooldridge, A. Atreya, *Combust Flame* 137 (2004) 351–365.
[4] B. Lewis, G. von Elbe, *J Chem Phys* 2 (5) (1934) 283–290.
[5] H. Hu, J. Keck, Autoignition of adiabatically compressed combustible gas mixtures, SAE Technical paper 872110 (1987).
[6] A. Moghaddas, C. Bennett, K. Eisazadeh-Far, H. Metghalchi, *J Energy Resour Technol* 134 (2012) 022205.
[7] O. Askari, E. Mimmo, M. Ferrari, H. Metghalchi, *J Energy Res Technol* 139 (2017) 012204.
[8] H. Quintens, C. Strozzi, R. Zitoun, M. Bellenoue, *Flow Turbul Combust* 102 (2019) 735–755.
[9] J. Santner, S.S. Goldsborough, *Combust Flame* 209 (2019) 41–62.
[10] L. Kagan, G. Sivashinsky, *Proc Combust Inst* 34 (2013) 857–863.
[11] Q. Fan, Y. Qi, Y. Wang, Z. Wang, *Combust Flame* 212 (2020) 252–269.
[12] C. Xiouris, T. Ye, J. Jayachandran, F.N. Egolfopoulos, *Combust Flame* 163 (2016) 270–283.

Please cite this article as: R. Lawson, V. Gururajan and A. Movaghar et al., Autoignition of reacting mixtures at engine-relevant conditions using confined spherically expanding flames, Proceedings of the Combustion Institute, https://doi.org/10.1016/j.proci.2020.06.224

[13] A. Movaghar, R. Lawson, F.N. Egolfopoulos, *Combust Flame* 212 (2020) 79–92.
[14] A. Omari, L. Tartakovsky, *Combust Flame* 168 (2016) 127–137.
[15] V. Gururajan, F.N. Egolfopoulos, *Combust Flame* 209 (2019) 478–480.
[16] D. Goodwin, H.K. Moffat, R.L. Speth, Cantera: an object- oriented software toolkit for chemical kinetics, thermodynamics, and transport processes, https://www.cantera.org (2017). Version 2.3.0.
[17] Z. Zhao, M. Chaos, A. Kazakov, F.L. Dryer, *Int J Chem Kinet* 40 (2008) 1–18.
[18] D. Bradley, P.H. Gaskell, X.J. Gu, *Combust Flame* 104 (1996) 176–198.
[19] R.J. Kee, L.R. Petzold, *A differential/algebraic equation formulation of the method-of-lines solution to systems of partial differential equations*, Sandia National Laboratories, 1986 In Technical Report SAND86–8893.
[20] D.B. Spalding, P.L. Stephenson, R.G. Taylor, *Combust Flame* 17 (1971) 55–64.
[21] G. Dixon-Lewis, I.G. Shepherd, *Symp (Int.) Combust.* 15 (1975) 1483–1491.
[22] R. Stauch, S. Lipp, U. Maas, *Combust Flame* 145 (2006) 533–542.
[23] S.Y. Cho, R.A. Yetter, F.L. Dryer, *Comput Phys* 102 (1992) 160–179.
[24] R.D. Richtmyer, K.W. Morton, *Difference Methods for Initial-Value Problems*, 2 ed., Interscience, New York, 1967.
[25] A.C. Hindmarsh, P.N. Brown, K.E. Grant, S.L. Lee, R. Serban, D.E. Shumaker, C.S. Woodward, *ACM Trans Math Softw* 31 (2005) 363–396.
[26] http://poli5.usc.edu:3000/USC/LTORC (2019).
[27] R.J. Kee, J.F. Grcar, M.D. Smooke, J.A. Miller, *Premix: a FORTRAN program for modeling steady laminar one-dimensional premixed flames*, Sandia National Laboratories, 1985 Sandia Report, SAND85-8240.
[28] G. Jomaas, C.K. Law, J.K. Bechtold, *J Fluid Mech* 583 (2007) 1–26.
[29] G.H. Markstein, *J Aeronaut Sci* 18 (1951) 199–209.
[30] G. Rozenchan, D.L. Zhu, C.K. Law, S.D. Tse, *Proc Combust Inst* 29 (2002) 1461–1470.
[31] J. Jayachandran, F.N. Egolfopoulos, *Proc Combust Inst* 36 (2017) 1505–1511.
[32] H. Yu, Z. Chen, *Combust Flame* 162 (2015) 4102–4111.
[33] A. Rodriguez, O. Frottier, O. Herbinet, R. Fournet, R. Bounaceur, C. Fittschen, F. Battin-Leclerc, *J Phys Chem A* 119 (2015) 7905–7923.
[34] U. Burke, K.P. Somers, P. O'Toole, C.M. Zinner, N. Marquet, G. Bourque, E.L. Petersen, W.K. Metcalfe, Z. Serinyel, H.J. Curran, *Combust Flame* 162 (2015) 315–330.
[35] Y. Ju, C.B. Reuter, S.H. Won, *Combust Flame* 162 (2015) 3580–3588.
[36] S.S. Merchant, C.F. Goldsmith, A.G. Vandeputte, M.P. Burke, S.J. Klippenstein, W.H. Green, *Combust Flame* 162 (2015) 3658–3673.
[37] V. Gururajan, F.N. Egolfopoulos, *Proc Combust Inst* 36 (2017) 4165–4174.

Please cite this article as: R. Lawson, V. Gururajan and A. Movaghar et al., Autoignition of reacting mixtures at engine-relevant conditions using confined spherically expanding flames, Proceedings of the Combustion Institute, https://doi.org/10.1016/j.proci.2020.06.224